ADVANCED MATERIALS INTERFACES
www.advmatinterfaces.de

Van der Waals Epitaxy of HgCdTe Thin Films for Flexible Infrared Optoelectronics

Wenwu Pan, Zekai Zhang, Renjie Gu, Shuo Ma, Lorenzo Faraone, and Wen Lei**

Van der Waals epitaxial (vdW) growth of semiconductor thin films on 2D layered substrates has recently attracted considerable attention since it provides a potential pathway for realizing monolithically integrated devices and flexible devices. In this work, direct growth of epitaxial HgCdTe (111) thin films on 2D layered transparent mica substrates is achieved via molecular beam epitaxy. The full width at half maximum of the ω-mode X-ray diffraction peak is measured to be around 306 arc sec. Mid-wave infrared photoconductors based on the as-grown HgCdTe thin films have been demonstrated and the self-heating effect has been evaluated. A peak responsivity at the wavelength of around 3500 nm is measured to be about 110 V W^{-1} at 80 K and 8 V W^{-1} at room temperature under a bias of 25 V cm^{-1}. Twinning defects are observed, limiting the crystallinity and mobility-lifetime product in HgCdTe/mica. Benefiting from the vdW epitaxial growth, an etch-free layer transfer process for lifting off the HgCdTe from the mica substrate has been demonstrated, leading to large area free-standing HgCdTe thin films.

1. Introduction

The detection of infrared (IR) radiation has a wide range of applications, including medical diagnosis, night vision, remote sensing, and defense technology. Thermal radiation falls within the atmospheric transmission windows of either the mid-wave infrared (3–5 µm, mid-wave infrared (MWIR)) band or the long-wave infrared (8–12 µm, LWIR) band. Commercial IR detectors working in these spectral bands have been developed over the years, including thermal detectors such as bolometers as well as narrow bandgap semiconductor photodetectors (≈0.25 and ≈0.1 eV, respectively, for MWIR and LWIR) including InSb, HgCdTe, or type-II superlattices.[1] Due to their unsurpassed performance, such as fast response, tailorable bandgap over the 1–30 µm range, and high quantum efficiency, HgCdTe-based IR photodetectors grown on lattice-matched $Cd_{0.96}Zn_{0.04}Te$ (CZT) substrates and associated focal plane arrays (FPAs) dominate the high-performance end of IR applications.[1]

The further development of IR applications requires the future HgCdTe IR detectors to have new features of lower cost, larger array format size, higher operating temperature, larger field of view (FOV), and multiband detection.[2] Over the past 10–20 years, significant progress has been achieved in these areas. For example, alternative substrates (Si, Ge, GaAs, and GaSb) instead of the traditional CZT substrates were researched for growing HgCdTe IR materials in order to fabricate next-generation IR imaging FPAs with lower cost and larger array format.[3–5] Recently curved imaging FPAs have been proposed as a feasible approach for achieving larger FOV with simpler and flatter lenses in comparison to conventional planer FPAs.[2] The conventional development pathway of these curved imaging FPAs relies on substrate thinning and FPA bending, which is inherently limited due to complex device processing, low yield, and high cost. Note that II–VI HgCdTe materials are more vulnerable to damage during the substrate-thinning processes because they are much more fragile and sensitive to chemical/mechanical damage in comparison to conventional Group IV and III–V semiconductors. In addition, the process does not remove the substrate completely due to the variability limits of array alignment on the polishing tool. Consequently, both the flexibility of the thinned FPA and the feasibility of monolithic integration are also limited in comparison to what could be achieved if transferable and/or free-standing HgCdTe device active layer of thickness <10 µm was available.

Two-dimensional (2D)-layered materials such as graphene and mica have the potential to serve as substrates for growing high-quality three-dimensional (3D) semiconductor thin films through van der Waals epitaxy (vdWE) techniques such as molecular beam epitaxy (MBE) and MOCVD.[6] For vdWE growth, the stringent requirement of matched lattice constants for high-quality heterostructure growth in traditional semiconductor epitaxy is mitigated. This is because the 2D-layered substrates have naturally passivated surfaces and strong chemical bonding is not required at the interface. In this way, the generation of dislocations at the interface can be effectively suppressed.[7,8]

W. Pan, Z. Zhang, R. Gu, S. Ma, L. Faraone, W. Lei
Department of Electrical
Electronic and Computer Engineering and ARC Centre of Excellence on Transformative Meta-Optical Systems (TMOS)
The University of Western Australia
35 Stirling Highway, Perth, WA 6009, Australia
E-mail: wenwu.pan@uwa.edu.au; wen.lei@uwa.edu.au

The ORCID identification number(s) for the author(s) of this article can be found under https://doi.org/10.1002/admi.202201932.

DOI: 10.1002/admi.202201932

In addition, benefiting from the weak out-of-plane bonding between 3D/2D interfaces, epitaxial layers can be easily lifted off and transferred, thus opening up new opportunities for fabricating flexible/monolithically integrated semiconductor devices for industry applications.[6,9,10] Significant research advances have been achieved in this area recently, with much of the work reported on Group IV, III–V, and binary II–VI semiconductors as well as associated optoelectronic devices working in the spectral range of from the visible band to near-infrared band.[6,9,10] Considering the great potential for optoelectronic applications in the MWIR and LWIR, there is a strong incentive to develop vdWE-assisted growth of HgCdTe and demonstrate its potential in layer lift-off/transfer to achieve ultrathin and flexible HgCdTe layers for subsequent shaping into curved IR imaging arrays.

The growth of single-crystal HgCdTe films on muscovite mica by a subsequent EDICT (evaporation and diffusion at constant temperature) treatment of the CdTe films at around 500 °C was reported in 1983.[11] However, due to their poor thermal stability, the mica substrates began to decompose and react with HgCdTe at that high temperature; consequently, the HgCdTe films were not entirely satisfactory for making devices and layer transfer.[11] In this work, for the first time, we report the direct vdWE-assisted MBE growth of MWIR HgCdTe thin films on lattice-mismatched 2D-layered fluorphlogopite mica substrates. Fourier-transform infrared spectroscopy (FTIR), X-ray diffraction (XRD), transmission electron microscopy (TEM), and optoelectronic response measurement were undertaken to study the material quality of the grown HgCdTe layers. Benefiting from the weak bonding at the abrupt HgCdTe/mica interface achieved by the vdWE-MBE growth, an etch-free layer-transferring process for lifting off the HgCdTe thin film from the mica substrate has been demonstrated, which may represent a significantly less complex option for fabricating flexible/monolithically integrated semiconductor devices including curved IR imaging arrays.

2. Results and Discussion

IR transmission measurements were used to determine the cutoff wavelength for vdWE-MBE $Hg_{1-x}Cd_xTe$ grown on mica. **Figure 1**a shows the FTIR transmission spectrum at 300 K

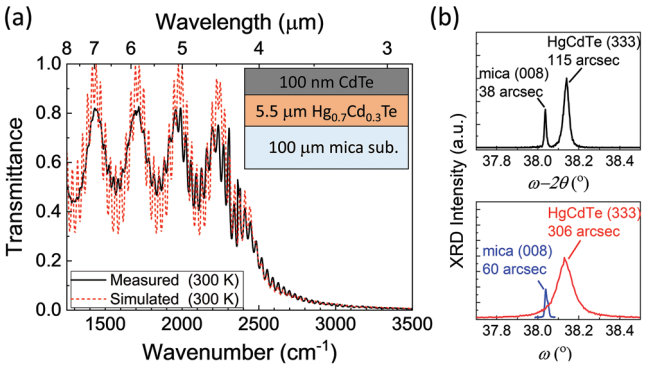

Figure 1. a) Experimental and modeled infrared transmission spectra at 300 K of a representative vdWE-MBE HgCdTe/mica sample. The inset illustrates the sample structure as extracted by simulation. b) HRXRD ω-2θ and ω scanning curves of a representative HgCdTe/mica sample.

of a typical HgCdTe thin film grown on mica, which presents an MWIR cutoff at around 4 μm. This suggests that $x = 0.3$ according to the bandgap relationship $E_g(x, T)$ for the $Hg_{1-x}Cd_xTe$ alloy.[12] Moreover, based on the optical interference fringes observed the thicknesses of the HgCdTe and mica substrate are determined to be ≈5.5 and ≈100 μm, respectively. Note that fluorphlogopite mica has excellent transmission (>80%) throughout the wavelength range from 350 nm to 8 μm,[13] which is favorable for back-illuminated IR detectors. The measured spectrum fits well with the simulated one, indicating a good composition uniformity along the growth direction for the MWIR HgCdTe sample.

Figure 1b shows the high-resolution X-ray diffraction (HRXRD) spectra of the vdWE-MBE grown MWIR HgCdTe. As denoted in Figure 1b, both the mica (008) peak and zinc-blende (ZB) HgCdTe (333) peak are observed in the ω-2θ spectrum, suggesting mica (001) can accommodate the growth of HgCdTe ZB (111) directly without a CdTe buffer ((008) and (333) are the same set of Miller planes as (001) and (111), respectively). Note that 2D-layered materials normally have hexagonal lattices, which can accommodate the growth of ZB (111) and/or wurtzite (WZ) (0001) easily because both of their in-plane lattices are hexagonal. The in-plane lattice parameters of $a = 4.58$ Å and $b = 7.93$ Å can be estimated for ZB-HgCdTe (111) considering the lattice constant of ZB-HgCdTe is around 6.47 Å.[14] This indicates a large in-plane lattice mismatch of 14% between the fluorphlogopite mica substrate ($a = 5.308$ Å, $b = 9.183$ Å) and the HgCdTe epilayer.[15] As shown in Figure 1b, an ω scan full width at half maximum (FWHM) (full width at half maximum) value of 306 arc sec is achieved for the direct growth of HgCdTe on mica, which is three- to five-times larger than that of (Hg)CdTe layers grown on conventional alternative substrates such as Si, Ge, GaAs, and GaSb, with state-of-the-art CdTe buffer layer technology.[3,16–18] Note that the relatively larger XRD FWHM measured for the HgCdTe on mica sample may be caused by imperfect cleavage of the mica substrate during substrate preparation prior to film growth, defects such as twins and dislocations generated during MBE growth, as well as substrate bowing due to its flexibility.

Figure 2a shows the cross-sectional TEM image of a representative vdWE-MBE grown HgCdTe showing a sharp interface with the mica substrate. As shown by the TEM image, the ZB-(111) HgCdTe has been grown with the formation of twinned domains, which are triggered by the ZB/WZ stacking fault. The formation of microtwins is commonly observed in HgCdTe grown with techniques such as MBE, in which (111) orientation is particularly vulnerable to twin formation.[19] Note that the ZB/WZ stacking fault in the (111) orientation growth requires very low formation energy, and can therefore occur several times during the growth. Further growth optimizations such as stringent controls of flux stability and substrate surface temperature are needed to address this twinning issue. The epitaxial relationships of HgCdTe on mica can be revealed from the selected area electron diffraction (SAED) pattern shown in Figure 2b: [$1\bar{2}1$] HgCdTe ‖ [010] mica and [111] HgCdTe ‖ [001] mica, which are consistent with the results of previous studies on other II–VI thin films grown on mica.[20]

Unlike conventional optoelectronic devices based on rigid substrates, the in-situ fabricated devices on flexible thin mica substrates have the great potential applications in flexible

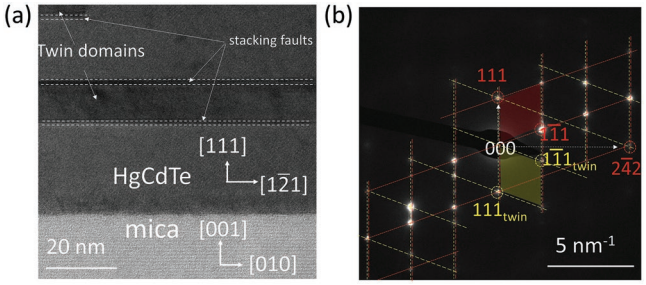

Figure 2. Structural properties of the vdWE-MBE grown HgCdTe on mica: a) HRTEM cross-sectional TEM image, and b) SAED pattern for the HgCdTe epilayer where twin domains are observed.

electronic devices such as cylindrically curved imager with 2π FOV.[21] To test this concept, at this early stage, it is essential to demonstrate the feasibility of device applications based on the as-grown HgCdTe on mica. **Figure 3**a shows the spectral responsivity (R_V) of the MWIR HgCdTe/mica photoconductor fabricated in this work, in which peak responsivity at the wavelength of around 3500 nm is measured to be ≈110 V W^{-1} at 80 K and ≈8 V W^{-1} at room temperature (RT). The spectral response cutoff wavelengths of ≈4.5 µm at 77 K and ≈4 µm at RT are consistent with the bandgap values of HgCdTe with x = 0.3. Note that the bias current (I_b) was adjusted with changing temperature (therefore the detector resistance, R) to keep the detector voltage ($V_b = I_bR$) at around 1 V (that is, at an electric filed strength of 25 V cm^{-1} considering the detector length is 400 µm) where either Joule heating or carrier sweep-out effects are negligible.

Note that MBE growth of HgCdTe typically produces a native hole concentration caused by Hg vacancies in the range of mid-10^{15} to low-10^{16} cm^{-3}.[19] The detector resistance can be expressed as $R = L/[eWt(n\mu_e + p\mu_h)]$ if surface conductance is neglected, in which e is electron charge, L, W, and t are the detector dimensions (length, width, and thickness, respectively), μ_e, μ_h are electron and hole mobilities ($\mu_e/\mu_h = 100$ is commonly assumed in HgCdTe),[22] and n, p are electron and hole concentrations. n, p can be given by $p = (p_0 + \sqrt{p_0^2 + 4n_i^2})/2$ and $n = n_i^2/p$,[23]

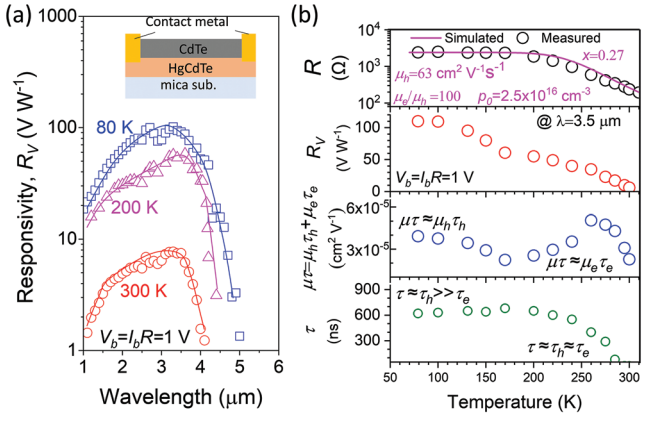

Figure 3. a) Measured photoresponse spectra of the fabricated HgCdTe detectors operating at 80, 200, and 300 K. b) Variation of photoconductor resistance (R), responsivity (R_V), effective mobility-lifetime product ($\mu\tau$), and carrier lifetime with temperature.

where n_i is the intrinsic carrier density and p_0 is the majority carrier hole concentration in p-type HgCdTe ($p \approx p_0$ when $p_0 >> n_i$). The device resistance can be approximated as $R \approx L/[eWt(p_0\mu_h + n_i^2\mu_e/p_0)]$. As shown in Figure 3b, the temperature-dependent detector resistance (R) shows two distinct regions. For temperatures above 200 K, the decrease in R with increasing temperature is mainly due to the fact that n_i is strongly temperature-dependent since $n_i \propto T^{3/2}\exp(-E_g/2kT)$,[24] where k is the Boltzmann constant. From the fitting (solid line in Figure 3b) for the measured device resistance, the x value in the HgCdTe is derived to be ≈0.27 and is lower than the FTIR-measured value of 0.3 as mentioned above. This would normally be ascribed to additional thermally activated defects in the HgCdTe layer,[25] which possibly tend to be ionized at high temperatures but were not considered in the fitting model. For temperatures below 200 K, the device resistance is relatively constant and appears to be determined by the extrinsic hole concentration with $R \approx L/(eWt\mu_h p_0)$ since $p_0 >> n_i$.

According to photoconductor theory,[26] the R_V can be expressed as $R_V = \lambda e\eta(\mu_e\tau_e + \mu_h\tau_h)I_bR^2/[hc(1+\beta)L^2]$, where λ is incident wavelength, η is quantum efficiency, τ_e, τ_h are electron and hole lifetimes, I_b is applied bias current, h is Planck's constant, c is the velocity of light, and β is a term-involving surface, bulk, and detector dimensions. β can be made negligible with the appropriate surface passivation and will be neglected hereafter. The quantum efficiency η can be calculated based on the formula: $\eta = (1-r)(1-e^{-\alpha t})/(1-re^{-\alpha t})$, where r is the reflectivity of the air/semiconductor interface and can be calculated as $r = [(1-n)/(1+n)]^2$, n is the refractive index, α is the absorption coefficient, and t is the thickness of HgCdTe. The expression for R_V can be simplified in two cases: (a) $R_V = \lambda e\eta\mu_e\tau_eI_bR^2/(hcL^2)$ for temperatures above about 200 K when $\tau_e \approx \tau_h$ and $\mu_e \gg \mu_h$, and (b) $R_V = \lambda e\eta\mu_h\tau_hI_bR^2/(hcL^2)$ for p-type materials at low temperatures in which electron trapping occurs ($\tau_e \ll \tau_h$).[27] Within the expression for R_V, it is important to note that the material quality should be evaluated by the effective carrier mobility-lifetime product $\mu\tau = \mu_e\tau_e + \mu_h\tau_h$ rather than by the R_V since it is strongly dependent on detector length L.

Based on the measured values of R and R_V as shown in Figure 2b, $\mu_h\tau_h$ is determined to be around 4×10^{-5} cm^2 V^{-1} for $T < 100$ K and the $\mu_e\tau_e$ is determined to be around 2×10^{-5} cm^2 V^{-1} at near RT. Using the carrier lifetime of $\tau_h \approx$ 600 ns measured for $T < 100$ K, the μ_h is estimated to be around 63 cm^2 V^{-1} S^{-1} (and therefore μ_e is estimated to be around 6300 cm^2 V^{-1} S^{-1} assuming μ_e/μ_h = 100) and the extrinsic hole density p_0 is calculated to be around 2.5×10^{16} cm^{-3}. Both the carrier mobilities and lifetime are typically an order of magnitude smaller than those of twin-free high-quality HgCdTe materials.[28] As a result, the responsivity of the fabricated HgCdTe/mica photoconductor is typically two orders of magnitude smaller than those of commercially available devices based on twin-free high-quality HgCdTe materials.[29] The $\mu\tau$ product can be optimized by reducing the formation of the observed twin structures in MBE growth, which generally act as carrier scattering/recombination defects and thus lead to reduced $\mu\tau$.

The expression of R_V for photoconductor responsivity shows that R_V increases monotonically with increasing bias if all other parameters including R remain constant. However, there are two important mechanisms that place practical limits on

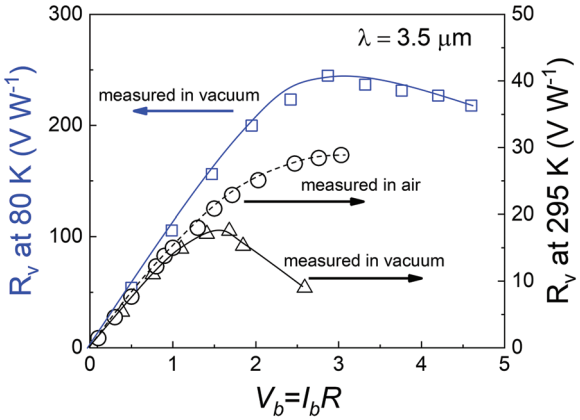

Figure 4. Measured responsivity at the wavelength of 3500 nm as a function of bias field. The circles represent data measured in air at 295 K, while the triangles and squares represent data measured in vacuum at temperatures of 295 and 80 K, respectively. The lines are a guide to the eye only.

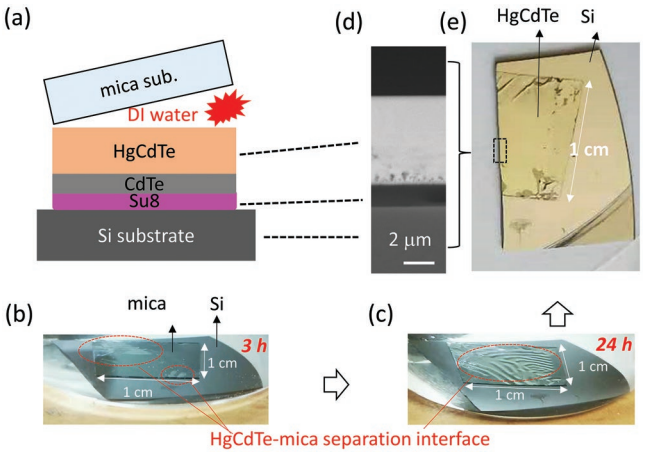

Figure 5. a–c) Illustration of the epilayer transfer process; d) Cross-sectional SEM image and e) optical image of HgCdTe membrane on photoresist/Si substrate after lifting off from the mica substrate.

the maximum allowable applied I_b and therefore V_b: (1) Joule heating of the detector element, which typically results in an increase of device temperature; (2) sweep-out of minority carriers, which needs to be considered if the excess carrier lifetime is long (typically > 1 μs) and the device is small (typically with dimensions < tens of μm). Note that, unlike conventional 3D semiconductors, 2D fluorphlogopite mica exhibits anisotropic behavior in terms of thermal conductivity. The reported value is ≈0.4 W m^{-1} K^{-1} for conductivity perpendicular to the planes, which is an order of magnitude lower than that parallel to the planes and other thermally isotropic 3D semiconductors.[30] Therefore, the self-heating effect is more likely to occur for a HgCdTe photoconductor on mica due to the relatively low thermal conductivity and hence, poor heat dissipation.

Figure 4 shows the variation of responsivity with bias field for the MWIR HgCdTe/mica detector operating at 80 K and RT. At low bias voltages, the responsivity increases almost linearly with increasing bias voltage. However, self-heating is observed at higher bias voltages since a decrease of detector resistance is observed, which limits the increasing responsivity. Under a vacuum environment, in comparison to the measurements at 80 K where the responsivity appears to saturate when $V_b > 3$ V ($I_b > 1$ mA), the self-heating effect is more significant at 300 K, which eventually causes the responsivity to fall when $V_b > 1.5$ V ($I_b > 5$ mA). This is to be expected since higher temperature results in lower detector resistance and higher self-heating power ($P_{sh} = I_b^2R = V_b^2/R$). For the device measured at RT, the self-heating effect can be reduced by having more efficient heat exchange in an air atmosphere than in vacuum. Further improvement of thermal conductivity can be achieved through thinning of the mica substrate or even transferring of the vdWE-MBE-grown HgCdTe films from mica substrates to some other target substrate for monolithic integration[31] and/or flexible optoelectronic applications, which can readily be achieved without the use of mechanical polishing or ion milling due to the benefit of the weak vdWE II–VI/mica interface force.

As depicted in **Figure 5**a, a feasible etch-free process for lifting off vdWE-MBE-grown HgCdTe films from mica substrates has been demonstrated. First, photoresist layers were coated on both surfaces of a CdTe/HgCdTe/mica sample and on the front surface of a foreign Si substrate. The photoresist edge was removed to expose the outer edges of the HgCdTe/mica. Then, the photoresist-coated surfaces were bonded and postbaked. The composite was then immersed in DI wafer. As shown by Figure 5b,c, because of the weak quasi-vdWE HgCdTe/mica interface, within a few hours water molecules can diffuse into the HgCdTe/mica interface, leading to the delamination of the mica substrate from the HgCdTe. As indicated by Figure 5d,e, in our preliminary experiment the successful transfer of the HgCdTe thin film with a size up to ≈1 cm^2 has been demonstrated. Eventually, the photoresist layers can be subsequently removed by dissolving in acetone. Although ultrasonic treatment and mechanical delamination can facilitate the lift-off process,[9] the 5.5 micron-thick HgCdTe thin films are found to be more vulnerable than much thinner films of other materials. To achieve a uniform and reproducible exfoliation of HgCdTe with a high yield for applications in low-cost flexible and/or monolithic-integrated infrared optoelectronic devices such as curved infrared imagers, the lift-off process needs to be optimized further, which is beyond the scope of this work.

3. Summary and Conclusions

To summarize, this work has demonstrated direct vdWE-MBE growth of MWIR HgCdTe thin films on mica and their application for infrared detectors. The vdWE-MBE-grown HgCdTe thin films are (111) oriented with a XRD FWHM of 306 arc sec. Twin defects typically associated with (111) growth are observed, which presumably limit the carrier mobility and lifetime for the as-grown HgCdTe. It has also been found that the self-heating effect needs to be considered for HgCdTe/mica detectors when high bias conditions are applied since mica is a poor heat conductor. Benefiting from the weak vdWE bonding between HgCdTe and the mica substrate, an etch-free layer lift-off/transfer process has been demonstrated that is capable of achieving ultrathin and flexible HgCdTe layers for fabricating curved IR imaging arrays in the future.

4. Experimental Section

The HgCdTe thin films were grown on 2D-layered fluorphlogopite mica [KMg3(AlSi3O10)F2] (001) substrates in a Riber 32P MBE system equipped with elementary Hg, Te, and compound CdTe as sources. A detailed description of the thermal cleaning process for the mica substrates prior to MBE growth could be found elsewhere.[9] A systematic study optimizing the HgCdTe growth on mica was carried out, which would be published elsewhere. The growth temperature of HgCdTe was around 185 °C, as indicated by a Gallium–Indium eutectic contact thermocouple. The growth surface was finished with a 100-nm thick CdTe-capping layer for surface protection and passivation. The beam equivalent pressure (BEP) was set to be 4×10^{-4} Torr for Hg, 1.5×10^{-6} Torr for Te, and 7×10^{-7} Torr for CdTe, corresponding to Hg-rich conditions with a growth rate of ≈2 μm h^{-1} for HgCdTe. The crystal structure/quality of HgCdTe films was examined by HRXRD (Panalytical Empyrean). The TEM imaging of the HgCdTe epilayers was carried out, with the specimens prepared by using a focused ion beam (FIB). The bandgap of HgCdTe films was determined by Fourier-transform infrared spectroscopy (FTIR) transmission. The responsivity spectra of HgCdTe photoconductors were measured by a grating spectrometer (Optronic Laboratories IR Spectroradiometer 756). For the fabrication of HgCdTe photoconductors, standard optical photolithography was used to define square mesas in sizes of $L = 400$ and $W = 1200$ μm. Finally, Cr/Au (10/200 nm) was deposited by thermal evaporation to form metallic contacts on the HgCdTe layer surface. The ohmic nature of the semiconductor/metal contact was confirmed by the observation of linear and symmetrical current–voltage (*I–V*) curves measured in darkness with temperature (*T*) ranging from 77 to 300 K, and the corresponding bias voltage (V_b) ranging from –1 to 1 V.

Acknowledgements

This work was supported by the Australian Research Council (grant Nos. DP200103188, DP170104562, LE170100233, and CE200100010), a Research Collaboration Award from the University of Western Australia and Curtin Faculty of SAE R&DC Small Grants 2022. Facilities used in this work were supported by the WA node of the Australian National Fabrication Facility (ANFF), and the Microscopy Australia Facility at the Centre for Microscopy, Characterization and Analysis (CMCA) at UWA. The authors thank Dr. Zakaria Quadir and Dr. X. Sun at John de Laeter Centre (JDLC) at Curtin University for their assistance with TEM experiments.

Conflict of Interest

The authors declare no conflict of interest.

Data Availability Statement

The data that support the findings of this study are available from the corresponding author upon reasonable request.

Keywords

flexible devices, HgCdTe, infrared optoelectronics, layer lift-off, mica, molecular beam epitaxy, van der Waals epitaxy

Received: September 7, 2022
Revised: October 25, 2022
Published online: December 4, 2022

[1] A. Rogalski, J. Antoszewski, L. Faraone, *J. Appl. Phys.* **2009**, *105*, 091101.
[2] D. Dumas, M. Fendler, F. Chemla, M. Cohen, P. Laporte, K. Tekaya, E. Le Coarer, J. Primot, H. Ribot, in: *High Energy, Optical, and Infrared Detectors for Astronomy V, International Society for Optics and Photonics,* Vol. *8453*, SPIE, **2012**, pp.518–529.
[3] W. Lei, R. J. Gu, J. Antoszewski, J. Dell, L. Faraone, *J. Electron. Mater.* **2014**, *43*, 2788.
[4] W. Lei, R. J. Gu, J. Antoszewski, J. Dell, G. Neusser, M. Sieger, B. Mizaikoff, L. Faraone, *J. Electron. Mater.* **2015**, *44*, 3180.
[5] W. W. Pan, R. J. Gu, Z. K. Zhang, W. Lei, G. A. Umana-Membreno, J. Antoszewski, L. Faraone, *J. Electron. Mater.* **2022**, *51*, 4869.
[6] H. Kum, D. Lee, W. Kong, H. Kim, Y. Park, Y. Kim, Y. Baek, S.-H. Bae, K. Lee, J. Kim, *Nat. Electron.* **2019**, *10*, 439.
[7] A. Koma, K. Sunouchi, T. Miyajima, *Fabrication of ultrathin heterostructures with van der Waals epitaxy*, American Vacuum Society, PhD diss. **1985**.
[8] A. Koma, *J. Cryst. Growth* **1999**, *201*, 236.
[9] W. Pan, J. Liu, Z. Zhang, R. Gu, A. Suvorova, S. Gain, H. Wang, Z. Li, L. Fu, L. Faraone, *Nano Res.* **2021**, *1*, 368.
[10] Q. Lian, X. Zhu, X. Wang, W. Bai, J. Yang, Y. Zhang, R. Qi, R. Huang, W. Hu, X. Tang, *Small* **2019**, *15*, 1900236.
[11] A. C. Greenwald, R. G. Wolfson, *HgCdTe Fabrication using Directed Energy Techniques*, Spire Corp, Bedford, MA **1981**.
[12] G. L. Hansen, J. L. Schmit, T. N. Casselman, *J. Appl. Phys.* **1982**, *53*, 7099.
[13] H. Peng, W. Dang, J. Cao, Y. Chen, D. Wu, W. Zheng, H. Li, Z.-X. Shen, Z. Liu, *Nat. Chem.* **2012**, *4*, 281.
[14] T. Skauli, T. Colin, *J. Cryst. Growth* **2001**, *222*, 719.
[15] J. W. McCauley, R. E. Newnham, G. V. Gibbs, *Am. Mineral.* **1973**, *58*, 249.
[16] W. Lei, Y. L. Ren, I. Madni, L. Faraone, *Infrared Phys. Technol.* **2018**, *92*, 96.
[17] W. W. Pan, R. J. Gu, Z. K. Zhang, J. L. Liu, W. Lei, L. Faraone, *J. Electron. Mater.* **2020**, *49*, 6983.
[18] W. Pan, S. K. Nath, S. Ma, R. Gu, Z. Zhang, L. Fu, L. Faraone, W. Lei, *J. Appl. Phys.* **2022**, *131*, 205304.
[19] J.-P. Faurie, *Prog. Cryst. Growth Charact. Mater.* **1994**, *29*, 85.
[20] Y. B. Yang, L. Seewald, D. Mohanty, Y. Wang, L. H. Zhang, K. Kisslinger, W. Xie, J. Shi, I. Bhat, S. Zhang, *Appl. Surf. Sci.* **2017**, *413*, 219.
[21] M. Yen, Y. Bitla, Y.-H. Chu, *Mater. Chem. Phys.* **2019**, *234*, 185.
[22] J. P. Rosbeck, R. E. Starr, S. L. Price, K. J. Riley, *J. Appl. Phys.* **1982**, *53*, 6430.
[23] D. A. Neamen, *Semiconductor Physics and Devices: Basic Principles*, McGraw-Hill, NY **2003**.
[24] G. L. Hansen, J. L. Schmit, *J. Appl. Phys.* **1983**, *54*, 1639.
[25] W.-D. Hu, X.-S. Chen, F. Yin, Z. J. Quan, Z. H. Ye, X. N. Hu, Z. F. Li, W. Lu, *J. Appl. Phys.* **2009**, *105*, 104502.
[26] R. L. Petritz, *Phys. Rev.* **1956**, *104*, 1508.
[27] F. D. Morten, R. E. J. King, *Appl. Optics* **1965**, *4*, 659.
[28] A. Rogalski, *Rep Prog Phys* **2005**, *68*, 2267.
[29] https://www.teledynejudson.com/products/photoconductive-mercury-cadmium-telluride-detectors (accessed: November 2022).
[30] A. S. Gray, C. Uher, *J. Mater. Sci.* **1977**, *12*, 959.
[31] C. Y. You, W. J. Deng, M. Liu, P. Zhou, B. X. An, B. Wang, S. L. Yu, Y. Z. Zhang, *IEEE Sens. J.* **2021**, *21*, 26708.